Water vapor intrusions into the High Arctic during winter

J. G. Doyle,[1] G. Lesins,[1] C. P. Thackray,[1] C. Perro,[1] G. J. Nott,[1] T. J. Duck,[1] R. Damoah,[2] and J. R. Drummond[1]

Received 18 March 2011; revised 10 May 2011; accepted 12 May 2011; published 29 June 2011.

[1] The meridional transport of water vapor into the High Arctic, accompanied by dry enthalpy and clouds, impacts the surface radiative forcing. The evolution of one such moist intrusion over 9–11 February 2010 is presented. The event is analyzed using a unique blend of measurements including a new pan-Arctic retrieval of column water vapor from the Microwave Humidity Sounders, water vapor profiles from a Raman lidar and a ground-based microwave radiometer at the Polar Environment Atmospheric Research Laboratory (PEARL), in Eureka (80°N, 86°W), on Ellesmere Island in the Canadian High Arctic. A radiation model reveals the intrusion is associated with a 17 W m^{-2} average increase in downwelling longwave irradiance. Optically thin clouds, as observed by the lidar, contribute a further 20 W m^{-2} to the downwelling longwave irradiance at their peak. Intrusion events are shown to be a regular occurrence in the Arctic winter with implications for the understanding of the mechanisms driving Arctic Amplification. **Citation:** Doyle, J. G., G. Lesins, C. P. Thackray, C. Perro, G. J. Nott, T. J. Duck, R. Damoah, and J. R. Drummond (2011), Water vapor intrusions into the High Arctic during winter, *Geophys. Res. Lett.*, *38*, L12806, doi:10.1029/2011GL047493.

1. Introduction

[2] In recent decades the Arctic has been warming considerably faster than the global average in a phenomenon referred to as Arctic Amplification [*Serreze and Francis*, 2006]. Several studies have provided evidence that enhanced meridional transport from the south may be a contributing factor [*Yang et al.*, 2010]. Meridional transport changes will impact the advection of dry enthalpy, water vapor (WV), and clouds into the Arctic where they can influence the radiative forcing at the surface. Although the High Arctic (latitudes > 70°N) winter atmosphere is extremely dry [*Lesins et al.*, 2010], WV contributes the most of all gases to longwave emission [*Curry et al.*, 1995], and creates supersaturations that maintain clouds with additional longwave forcing [*Shupe and Intrieri*, 2004]. This study investigates the surface radiative forcing associated with an increase in WV measured at the Polar Environment Atmospheric Research Laboratory (PEARL) at Eureka, Ellesmere Island (80°N, 86°W) from 9 to 11 February, 2010. Cases of WV advection into the High Arctic from the south are hereafter referred to as "intrusions."

[1]Department of Physics and Atmospheric Science, Dalhousie University, Halifax, Nova Scotia, Canada.
[2]Department of Earth and Environmental Sciences, University of Waterloo, Waterloo, Ontario, Canada.

Published in 2011 by the American Geophysical Union.

[3] Water vapor at Eureka is obtained from twice-daily radiosonde profiles, continuous precipitable water (PW) columns by microwave radiometer (MWR; 20% error in PW retrievals) [*Westwater et al.*, 2001], and continuous vertical profiles by the CANDAC (Canadian Network for the Detection of Atmospheric Change) Rayleigh-Mie-Raman Lidar (CRL) (G. J. Nott et al., A remotely-operated lidar for aerosol, temperature, and water vapor profiling in the High Arctic, submitted to the *Journal of Atmospheric and Oceanic Technology*, 2011). The CRL also provides simultaneous measurements of cloud and aerosol optical properties, critical to understanding the radiative environment.

[4] The Microwave Humidity Sounder (MHS) aboard the NOAA-18 and MetOp-A satellites is used to obtain PW across the entire Arctic without cloud or precipitation interference. MHS is the next generation instrument replacing the Advanced Microwave Sounding Unit B (AMSU-B). The AMSU-B retrieval of *Melsheimer and Heygster* [2008] was adapted to the improved radiometric performance and higher spatial resolution (17 km at nadir) of MHS during the winter months when PW is low enough to prevent saturation of the surface signal. The retrievals were validated against ten-minute average measurements from ground-based MWRs [*Westwater et al.*, 2001] at the ARM North slope Alaska site (not shown). The average difference was 0.4 mm of MHS-derived PW having a −0.17 mm bias compared to the surface radiometer.

[5] First the horizontal and vertical structure of the intrusion event is shown. The mid-latitude source of the moist airmass is confirmed using the FLEXTRA trajectory model [*Stohl et al.*, 1995]. Longwave contributions to the radiative forcing from different components are assessed using the Santa Barbara DISORT Atmospheric Radiative Transfer (SBDART) model (uncertainty ±3%) [*Ricchiazzi et al.*, 1998]. These are compared to irradiance measured by the pyrgeometer (uncertainty ±9 W m^{-2}) [*Augustine et al.*, 2000] located at Eureka, 5 km from the CRL on a tower standing 10 m above ground level. Finally, this intrusion is placed in context of an entire winter by examining the MWR-derived PW columns during four winters at Eureka.

2. Observations

2.1. Synoptic Situation

[6] On 6 February, the 500 hPa pressure level height in the western Arctic had a dipole pattern with low heights north of Alaska and high heights over Greenland. The surface analysis reveals a strong ridge of high pressure extending south from the North Pole into mainland Canada. South of Alaska, a deep but weakening low was moving north, and stalled by 7 February in southern Alaska. The warm air advection associated with the low pressure system carried

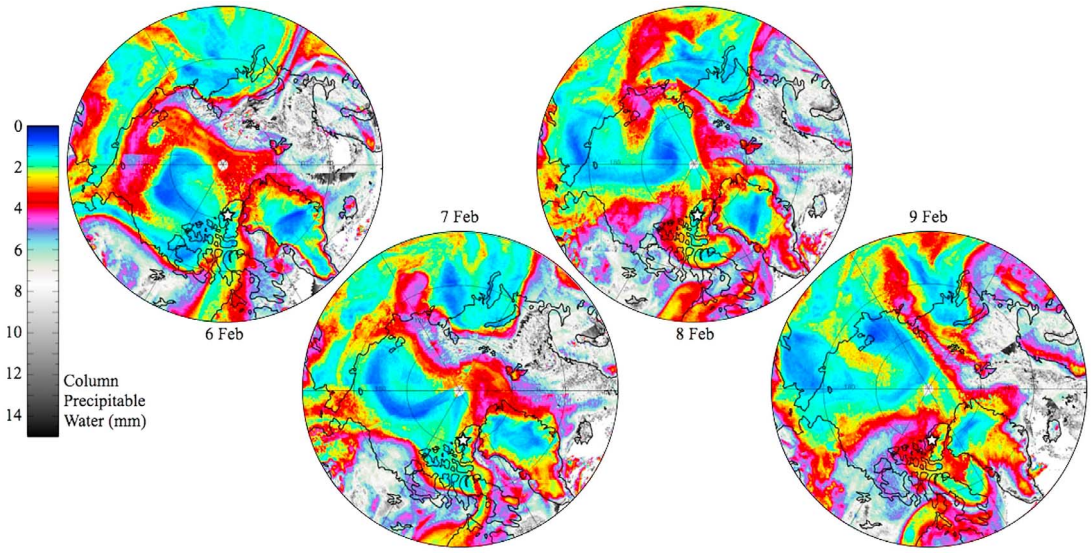

Figure 1. Pan-Arctic mosaic of PW calculated using two satellite (NOAA-18 and MetOp-A) based Microwave Humidity Sounders for 6–9 February, 2010. Eureka is marked with a star, with North America along the bottom and Russia along the top edge of the map. See Section 2.2 for description and Section 2.1 for synoptic details.

moisture north of the Canadian Arctic coast at 700 hPa. On 8 February this warm air advection towards Eureka was disrupted by a weak but developing 500 hPa low moving north-west from just west of Greenland to south of Eureka.

2.2. Microwave Humidity Sounder

[7] Pan-Arctic mosaics of MHS PW are shown in Figure 1 for 6–9 February 2010. Satellite swaths performed from 00:00 to 12:00 UTC were combined (usually seven) for each daily mosaic. Each mosaic is characterized by dry atmospheric conditions (PW < 2 mm; blue-green regions in Figure 1), with moist intrusions (PW > 3 mm; red-black regions), incoming from lower latitudes. On 6 February, the western Canadian Arctic Archipelago and Beaufort Sea was mostly dry, with moist air over mainland North America. Over the following three days, an intrusion of moist air originating from the Alaskan low advected from the mainland over the Beaufort Sea, eventually reaching the most northern part of the Archipelago and Eureka on 9 February. Further mosaics show the intrusion, blocked by a developing low to the south, remained stationary to the west of Eureka until 11 February.

[8] The MHS analysis allows tracking of column PW only. To identify the three-dimensional aspects of the intrusion, air parcel back trajectories were computed using the FLEXTRA model (not shown, see Figure S1 of the auxiliary material).[1] The FLEXTRA analysis reveals that the source region for the moisture in the intrusion was the Pacific Ocean. Furthermore, back trajectories corresponding to 500 and 1000 m trace over the north pole from Russia show a separation between the airmass in the free troposphere and the strong winter-time temperature inversion.

2.3. Lidar

[9] Figure 2 shows the time-height cross-section of WV mixing ratio measured by the CRL between 20:35 UTC 8 February and 12:52 UTC 11 February. Data is presented with 15 minute integration and 80, 150, 300 m vertical resolution between 0, 2.5, 4 and 10 km, respectively. Each day between 16:00 and 22:00 UTC, the missing data above 4 km is due to noise from scattered sunlight. The height of temperature inversions measured by the 00:00 and 12:00 UTC daily radiosondes are indicated by black plus (+) signs.

[10] Late on 8 February, the WV mixing ratio was at a background level of only 0.2 g kg^{-1} above the surface temperature inversion height of 900 m. Integrating the lidar profile gave a column depth of 1.6 mm which agrees well with the values seen by the MHS over Eureka at this time. The intrusion of moist air is seen arriving at about 4 km altitude at 03:00 UTC 9 February and then progressively lower to 600 m by 18:00 UTC, hereafter referred to as period "A". The intrusion reached a peak WV mixing ratio of 1.66 g kg^{-1} (statistical uncertainty ±0.06) at 16:14 UTC 9 February. Although most of the moist air remained above the surface inversion, some was present in the boundary layer between 16:00 UTC 9 February and 04:00 UTC 10 February. The surface inversion layer appears to limit the further lowering of the enhanced WV.

[11] The intrusion retreated west of Eureka by 05:00 UTC 10 February, leaving dry air above 2.2 km. This dryer period is referred to as "B". Based on MHS analysis (not shown), the original intrusion re-advanced by 12:00 UTC 10 February, giving the appearance of a second intrusion in the lidar data (Figure 2). This re-advancement is referred to as period "C", and was confined between 2 and 4 km altitude. From the radiosonde profiles, the top of the surface temperature inversion in periods B and C was at approximately 2 km and appears to separate the re-advanced moisture from the residual moisture below.

2.4. Pyrgeometer

[12] Downwelling longwave irradiance as measured by the pyrgeometer over the period of the CRL observation is shown as the black line in Figure 3. Changes in irradiance

[1] Auxiliary materials are available in the HTML. doi:10.1029/2011GL047493.

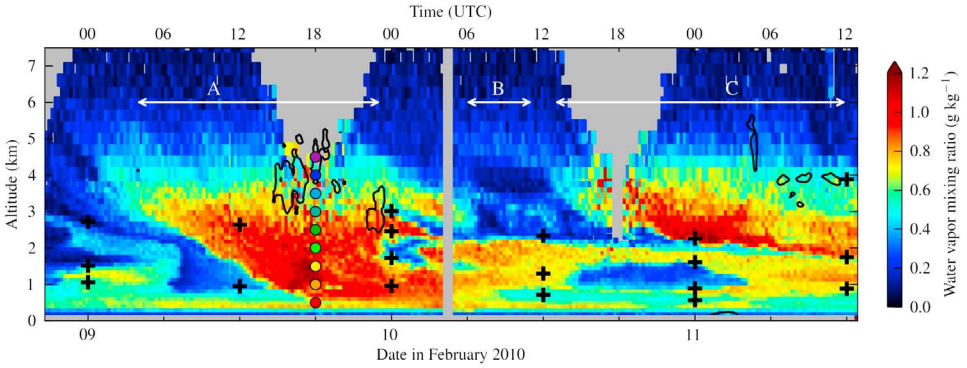

Figure 2. Lidar-measured water vapor mixing ratio (g kg^{-1}) over Eureka, Nunavut beginning at 20:35 UTC 8 February, 2010 and ending at 12:52 UTC 11 February. Grey indicates data with statistical uncertainty over 100% and the vertical grey bar indicates no data. Colored circles at 18:00 UTC 9 February correspond to the starting time and altitudes of the FLEXTRA back trajectories. Clouds observed by the CRL are traced in black. Black crosses indicate temperature inversion altitudes, measured by radiosonde.

from the beginning of the measurement are presented to minimize any bias due to local temperature uncertainty and possible frosting on the instrument. During period A, the radiation increased to a maximum of 54 W m^{-2} at 15:40 UTC 9 February, which is associated with the maximum of WV seen in the lidar data, as well as the presence of clouds (outlined in black in Figure 2). The downwelling radiation decreased between 00:00 and 16:00 UTC 10 February. This corresponded to the influx of dry air above 2.2 km during period B. After 16:00 UTC 10 February, the downwelling radiation increased again due to the second pulse of moist air above 2 km (period C). The intrusion was associated with an average measured increase of 16 W m^{-2} in downward longwave irradiance.

3. Modeling

[13] The SBDART radiative transfer model was used to simulate the downward longwave radiation at the surface and to compute the irradiance deviations of the contributing factors in the intrusion. Continuous WV mixing ratio profiles measured by the CRL (data with statistical uncertainty greater than 50% were masked), with temperature profiles interpolated between 12-hour radiosondes were used as model input. A constant ozone density profile was assumed, using an ozonesonde launched at 23 UTC 10 February from Eureka. Cloud-bottom and -top heights and optical depth were obtained from the lidar measurements. Cloud outlines as determined for a backscatter coefficient threshold of 1.1 × 10^{-5} m sr^{-1} are shown superimposed on the WV mixing ratio in Figure 2. The clouds were specified as ice particles with an effective radius of 60 μm [*Bourdages et al.*, 2009], although the irradiance is relatively insensitive to the effective radius with less than 1% variation for radii 25–120 μm.

[14] Figure 3 shows the simulated change in downwelling longwave irradiance (grey line). Temporal variation in the simulated irradiance agrees well with that of the observations (black line), with most of the fluctuations due to clouds being captured. Some discrepancies are seen in the cloud contributions at 06:00 and 09:00 UTC 11 February. This is likely due to the pyrgeometer measurements being influenced by clouds over the entire sky whereas the model uses the zenith-pointing lidar profiles. An average increase in irradiance during the intrusion of 17 W m^{-2} was simulated, which is in agreement with the pyrgeometer measurement.

[15] The downwelling longwave radiation simulated without the cloud component is shown in Figure 3 (green line). During period A when the majority of the WV arrived, the cloud-free simulation indicates a 22 W m^{-2} increase in downwelling radiation. According to the simulation, the cloud arriving at 15:40 UTC 9 February has an additional positive contribution of 20 W m^{-2} to the downward radiation. The average cloud contribution for the case study was calculated to be 9 W m^{-2}.

[16] The increase seen in the cloud-free simulation is a combination of the higher WV concentration and warmer temperatures associated with the intrusion. Two control cases were simulated to assess the relative contributions of WV concentration and temperature to the enhanced clear sky downwelling radiation. First, the WV is fixed to the initial profile while the temperature varied (red line), then the temperature is fixed and the WV varied (blue line).

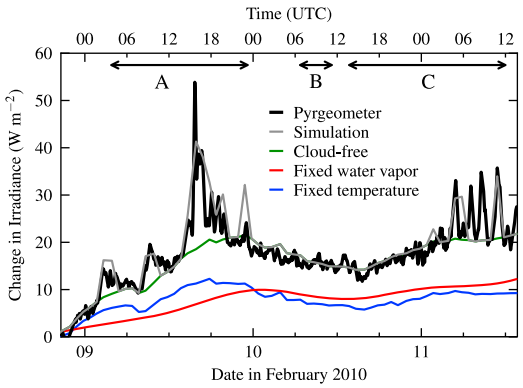

Figure 3. Change in downwelling radiation (W m^{-2}) over Eureka beginning at 20:35 UTC 8 February, 2010 and ending at 12:52 UTC 11 February. Modelled results using lidar data shown in Figure 2, radiosonde and ozonesonde profiles as input are shown in grey. Cloud-free, fixed water vapor and fixed temperature control simulations are shown in green, red and blue respectively. Pyrgeometer measurements at Eureka are shown in black.

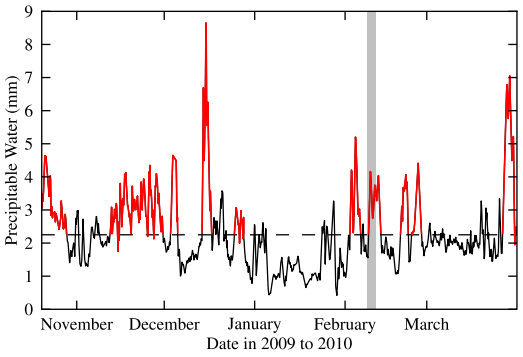

Figure 4. Total column PW from 20 October, 2009 to 31 March, 2010 measured by the MWR in Eureka. Data is presented with 3 hour averaging. The dashed line indicates the average PW during the 2007–2011 winters. Intrusions are indicated by red lines (see Section 4). The vertical grey bar corresponds to the time of the lidar observation in Figure 2.

[17] As the moist air descended to lower and warmer altitudes (period A), the relative contribution of WV to downwelling radiation increased more rapidly than the contribution from temperature. Drier air then moved in above 2.2 km (period B) and the relative contribution of WV consequently decreased while the contribution of temperature continued to increase. At the time of the re-advancement of the intrusion (period C) the WV component of the downward radiation fluctuation once again increased. On average over the entire measurement time period, the cloud-free simulations indicate approximately equal contributions to the downward longwave radiation from the temperature and WV increases.

4. Intrusion Frequency

[18] In order to determine the significance of the intrusions in this specific case study as well as in general during the Arctic winter, the instances of WV intrusions were obtained from 3-hour average MWR measurements of PW at Eureka for winters from 2007 to 2011. As an example, Figure 4 shows the PW from the winter of 2009 to 2010, with the time corresponding to the presented case study indicated in grey.

[19] To identify an intrusion, a baseline of PW was established by averaging data from all four winters (shown as a dotted line in Figure 4 at 2.3 mm). Periods of enhanced water vapour are defined by PW greater than the climatological baseline for longer than 6 hours. To characterize the significance of such an enhancement, the PW was integrated over the duration. By inspection, intrusions were defined as periods of enhanced WV with an integrated PW greater than 5.5 mm day, corresponding to 34% of the enhancements. The choice of 5.5 mm day corresponds to a natural separation in the distribution of integrated PW, although the significance of this is unknown (not shown, see Figure S2).

[20] Using this definition, 29 intrusions are identified during the winters of 2007 to 2011, occurring 30% of the observed time. The 10 intrusions that occurred during the winter of 2009 to 2010 are shown in Figure 4 in red. The average intrusion persists for 132 hours with PW peaking at 5.2 mm. Clear sky downwelling irradiance is modelled during the same winters with SBDART, using interpolated radiosonde WV, temperature, and ozone profiles as inputs. From this the average intrusion was determined to be accompanied by a 19 W m^{-2} increase of downwelling radiation from the climatological baseline of 138 W m^{-2}. The integrated PW for each period of enhanced WV and corresponding irradiance is included in the auxiliary material for comparison.

[21] To determine if the 9–11 February intrusion pathway is typical of all the intrusions, pan-Arctic MHS mosaics from 1 January to 31 March, 2010 were inspected. Not surprisingly the flows carrying appreciable water vapour were either from the Pacific, moving north-east over Alaska or north-west over Siberia; or from the Atlantic, either arriving at Eureka directly from the south-east or moving into the Arctic to the east of Greenland then curling around and reaching Eureka from the north.

5. Conclusion

[22] A case study has been presented of an intrusion of WV from the northern Pacific Ocean into the High Arctic. By combining MHS PW mosaics and Raman lidar WV mixing ratio profiles, a new perspective is obtained on the movement and evolution of WV during such events. The event increased the WV mixing ratio from a background level around 0.2 g kg^{-1} to a maximum of 1.66 g kg^{-1} and remained above 0.8 g kg^{-1} for the duration of the measurement. This intrusion was accompanied by an average increase in downward longwave irradiance at the surface of 16 W m^{-2} with an additional 9 W m^{-2} forcing from clouds.

[23] A climatological baseline of PW was determined from four winters of microwave radiometer measurements and based on this, 29 intrusions were counted between 2007 and 2011. Intrusions accounted for 30% of the winter periods. On average, an intrusion over Eureka lasts 132 hours and increases the PW by 5.2 mm and clear sky longwave downwelling irradiance by 19 W m^{-2} above their baseline values.

[24] The frequent occurrence of WV intrusions and the substantial impact they have on the surface radiation have important implications for the energetics of the winter-time Arctic. Although the intrusion studied here was accompanied by very little cloud and no surface precipitation, this situation is likely common in the High Arctic where the subsidence associated with the polar meridional cell inhibits significant cloud formation. Nevertheless, even relatively small cloud optical depths provide significant enhancements to the downward longwave irradiance. This case study—presented in terms of horizontal and vertical structure, effect on radiation, and seasonal significance—illustrates the importance of WV intrusions into the winter-time Arctic, when the background levels of PW are very low.

[25] **Acknowledgments.** The Polar Environment Atmospheric Research Laboratory (PEARL) is operated by the Canadian Network for the Detection of Atmospheric Change (CANDAC). CANDAC/PEARL funding partners are: the Arctic Research Infrastructure Fund, Atlantic Innovation Fund/Nova Scotia Research Innovation Trust, Canadian Foundation for Climate and Atmospheric Science, Canadian Foundation for Innovation, Canadian Space Agency, Environment Canada, Government of Canada International Polar Year, Natural Sciences and Engineering Research Council, Ontario Innovation Trust, Ontario Research Fund, Indian and Northern Affairs Canada, and the Polar Continental Shelf Program. The authors thank Taneil Uttal and R. Albee from NOAA for the flux tower in Eureka and the pyrgeometer data used. We also thank

NOAA-CLASS for making the MHS data available and NOAA-SEARCH for the MWR data. Finally, we thank ECMWF for providing the ERA Interim data.

[26] The Editor thanks the two anonymous reviewers for their assistance in evaluating this paper.

References

Alexeev, V. A., P. L. Langen, and J. R. Bates (2005), Polar amplification of surface warming on an aquaplanet in "ghost forcing" experiments without sea ice feedbacks, *Clim. Dyn.*, *24*(7), 655–666, doi:10.1007/s00382-005-0018-3.

Augustine, J. A., J. J. DeLuisi, and C. N. Long (2000), SURFRAD—A national surface radiation budget network for atmospheric research, *Bull. Am. Meteorol. Soc.*, *81*(10), 2341–2357, doi:10.1175/1520-0477(2000)081<2341:SANSRB>2.3.CO;2.

Bourdages, L., T. J. Duck, G. Lesins, J. R. Drummond, and E. W. Eloranta (2009), Physical properties of High Arctic tropospheric particles during winter, *Atmos. Chem. Phys.*, *9*, 6881–6897, doi:10.5194/acp-9-6881-2009.

Curry, J. A., J. L. Schramm, M. C. Serreze, and E. E. Ebert (1995), Water vapor feedback over the Arctic Ocean, *J. Geophys. Res.*, *100*(D7), 14,223–14,229, doi:10.1029/95JD00824.

Lesins, G., T. J. Duck, and J. R. Drummond (2010), Climate trends at Eureka in the Canadian High Arctic, *Atmos. Ocean*, *48*(2), 59–80, doi:10.3137/AO1103.2010.

Melsheimer, C., and G. Heygster (2008), Improved retrieval of total water vapor over polar regions from AMSU-B microwave radiometer data, *IEEE Geosci. Remote Sens.*, *46*(8), 2307–2322, doi:10.1109/TGRS.2008.918013.

Ricchiazzi, P., S. Yang, C. Gautier, and D. Sowle (1998), SBDART: A research and teaching software tool for plane-parallel radiative transfer in the Earth's atmosphere, *Bull. Am. Meteorol. Soc.*, *79*(10), 2101–2114, doi:10.1175/1520-0477(1998)079<2101:SARATS>2.0.CO;2.

Serreze, M. C., and J. A. Francis (2006), The Arctic amplification debate, *Clim. Change*, *76*(3–4), 241–264, doi:10.1007/s10584-005-9017-y.

Shupe, M. D., and J. M. Intrieri (2004), Cloud radiative forcing of the Arctic surface: The influence of cloud properties, surface albedo, and solar zenith angle, *J. Clim.*, *17*(3), 616–628, doi:10.1175/1520-0442(2004)017<0616:CRFOTA>2.0.CO;2.

Stohl, A., G. Wotawa, P. Seibert, and H. Kromp-Kolb (1995), Interpolation errors in wind fields as a function of spatial and temporal resolution and their impact on different types of kinematic trajectories, *J. Appl. Meteorol.*, *34*(10), 2149–2165, doi:10.1175/1520-0450(1995)034<2149:IEIWFA>2.0.CO;2.

Westwater, E. R., Y. Han, M. D. Shupe, and S. Y. Matrosov (2001), Analysis of integrated cloud liquid and precipitable water vapor retrievals from microwave radiometers during the Surface Heat Budget of the Arctic Ocean project, *J. Geophys. Res.*, *106*, 32,019–32,030, doi:10.1029/2000JD000055.

Yang, X.-Y., J. C. Fyfe, and G. M. Flato (2010), The role of poleward energy transport in Arctic temperature evolution, *Geophys. Res. Lett.*, *37*, L14803, doi:10.1029/2010GL043934.

R. Damoah, Centre for Atmospheric Sciences, Department of Earth and Environmental Sciences, University of Waterloo, 200 University Ave. West, Waterloo, ON N2L 3G1, Canada. (rdamoah@uwaterloo.ca)

J. G. Doyle, J. R. Drummond, T. J. Duck, G. Lesins, G. J. Nott, C. Perro, and C. P. Thackray, Department of Physics and Atmospheric Science, Dalhousie University, Dunn Building, Halifax, NS B3H 3J5, Canada. (doylejg@dal.ca; tom.duck@dal.ca)